Received: 11 March 2020 | Revised: 23 October 2020 | Accepted: 30 November 2020

DOI: 10.1002/we.2602

WILEY

RESEARCH ARTICLE

A comparative study on the dynamic behaviour of 10 MW conventional and compact gearboxes for offshore wind turbines

Shuaishuai Wang[1] | Amir Nejad[1] | Erin E. Bachynski[1,2] | Torgeir Moan[1,2]

[1]Department of Marine Technology, Norwegian University of Science and Technology, Trondheim, Norway

[2]Center of Autonomous Marine Operations and Systems (AMOS), Norwegian University of Science and Technology, Trondheim, Norway

Correspondence
Shuaishuai Wang, Department of Marine Technology, Norwegian University of Science and Technology (NTNU), Trondheim NO-7491, Norway.
Email: shuaishuai.wang@ntnu.no

Funding information
China Scholarship Council, Grant/Award Number: 201706050147

Abstract

This study compares the dynamic behaviour of a conventional and a compact gearbox for the DTU 10 MW wind turbine supported on a monopile offshore structure. The conventional gearbox configuration is composed of two planetary epicyclic stages and one parallel stage, while the compact gearbox configuration consists of a fixed planetary stage and a differential compound epicyclic stage. The design methodology for these two gearboxes is described, and the final gearbox specifications show a lighter weight and smaller volume for the compact gearbox design compared to the conventional one. Computational gearbox models are established using the multi-body system dynamic analysis method. A decoupled approach is employed for the gearbox load effect analysis. Comparisons of the dynamic behaviour between these two gearboxes are conducted under pure torque load cases, tangential pin position error conditions and non-torque load cases. The results demonstrate that the compact gearbox has better dynamic performance under different torque load cases and is more robust to withstand the effects of manufacturing errors and rotor non-torque loads compared to the conventional gearbox. It is believed that the proposed compact gearbox concept is promising and would be a good alternative for multi-megawatt floating wind turbines, although challenging with respect to the design and operation complexity.

KEYWORDS

10 MW gearbox, conventional and compact layouts, dynamic behaviour, offshore wind turbines

1 | INTRODUCTION

As the wind industry moves toward deeper ocean sites, there is a trend to up-scale the wind turbine size. The drivetrain is the core unit of wind turbines and is closely related to the wind power costs. Two basic configurations, namely, a geared high-speed drivetrain and a direct-driven drivetrain, are typically used. It is not clear what is the optimal choice. Moreover, the operational environment as well as the installation and maintenance costs for the drivetrain in offshore sites differs significantly from onshore sites. Based on these considerations, medium-speed drivetrain concepts have been emerging on the market, in order to lower the gearbox failure risk compared to the high-speed drivetain and to reduce the

weight and cost of the generator compared to a direct-driven drivetrain. One representative medium-speed drivetrain concept was proposed by the Technical University of Denmark (DTU) in 2013,[1] but DTU only published very general parameters for the drivetrain design. To facilitate the research on dynamics of the 10 MW wind turbine, a detailed drivetain model was designed by Wang et al.[2,3] This detailed, openly available, drivetrain model adopts a traditional three-stage gearbox design.

To alleviate the high cost of transportation, lifting and installation for the drivetrain in large-scale offshore wind turbines, a light-weight design of the drivetrain is essential. One good solution is to reduce the gearbox weight by using novel layouts, such as power split and compound planet gear transmission, to replace the conventional serial power transmission layout. In practice, while these novel gearbox layouts have been attempted, such as Areva's 5 MW[4] and Vestas' 9.5 MW[5] wind turbines, they have not been widely used in the market. This is because the structure of such novel gearboxes is more complex, making them more difficult to manufacture and assemble compared to conventional gearboxes. In addition, the novel gearbox may pose more challenge for inspection, maintenance and repair due to the reduction in available space. Further design and analysis efforts are hence needed to assess the novel gearbox design.

In order to reduce the gearbox weight and volume for the DTU 10 MW wind turbine, Wang et al.[6] designed a compact gearbox which adopted both power split and compound planet gear transmission technologies, resulting in a lighter weight and much smaller size than the conventional gearbox. However, some potential drawbacks of the compact gearbox were also demonstrated. High-precision gear design, manufacturing and installation are required to mitigate the imbalance of forces or moments among different components inside the gearbox. Moreover, compared to the conventional gearbox, the costs of inspection, maintenance and repair might be higher for the compact gearbox because the available space is narrower. Additionally, some specific components might be costly to produce, since they may need to be customized. Overall, considering transportation, lifting, inspection and maintenance, both the conventional and the compact gearboxes have their own advantages and disadvantages. However, the gearbox performance should be assessed from its whole life cycle perspective, in which the reliability assessment is a crucial part. Many studies on dynamic analysis of conventional gearboxes have been conducted (e.g., Guo et al.;[7] Helsen et al.;[8] Mo et al.;[9] Bhardwaj et al.[10]), while very limited information about the dynamic performance of the compact gearbox is available in the open literature.

The objective of this study is to compare the operational performance and dynamic behaviour of the conventional and the compact gearbox. Dynamic analysis of these two gearboxes is conducted and compared under multiple load cases and conditions of tangential pin position error, as a common manufacturing error in wind turbine gearboxes. This study contributes to a better understanding of the dynamic behaviour of conventional and compact gearboxes. The present work is a step forward in the use of novel drivetrains in large-scale offshore wind turbines.

2 | DESCRIPTION OF CONVENTIONAL AND COMPACT GEARBOX CONFIGURATIONS

Two gearbox configurations, as shown in Figure 1, are employed in this study. Their topology is illustrated in Figure 2. The conventional gearbox configuration consists of two planetary stages and one parallel stage, and the full power flows through these three stages serially. In contrast, the compact gearbox configuration is composed of one fixed planetary stage and one differential epicyclic stage, which correspond to the first stage and the second stage in the Figure 1B, respectively. The first stage is defined to the right side of the second stage, which opposite compared to the conventional gearbox, because the rotational speed of the output component, namely, the Sun gear, of the fixed planetary stage is lower than that of the differential epicyclic stage. Compared to the conventional gearbox, a main feature of the compact gearbox is that the full power is shared through two transmission paths simultaneously. Additionally, the second stage of the compact gearbox adopts compound epicyclic planet gear sets, by which a large gear transmission ratio is achieved. As a result, a compact gearbox size is realized. In the conventional gearbox, ring gears in the two planetary stages are part of the gearbox housing, and Sun gears adopt floating configurations. In contrast, in the compact gearbox, both Sun gears and ring gears of the two stages are set in floating configurations.

These two gearboxes are designed using the same design methodology, which is based on the international standard IEC 61400-4.[11] The design loads are defined as a load duration distribution (LDD) that consists of 64 load bins, obtained by post-processing the global simulation loads of the wind turbine over the whole normal operating range. Critical gearbox components—gears and bearings—are designed according to fatigue limit state criteria. More specifically, gears are designed based on the ISO 6336 series of design codes,[12-15] using the minimum safety factors recommended by IEC 61400-4[11] for gear tooth pitting resistance and bending strength. Bearings are designed based on the international standard ISO 281,[16] which describes the methods to evaluate the bearing dynamic load ratings and rating life. Bearing fatigue life is used to guide the bearing design. The detailed gearbox design process and design parameters can be found in the studies of Wang et al.[3,6]

Table 1 illustrates the general specifications of the conventional and the compact gearboxes. The compact gearbox volume, which is represented by the gearbox length and maximum gear outer diameter, is remarkably smaller than that of the conventional gearbox. Nonetheless, the total dry weight of the compact gearbox is not significantly lower than the conventional gearbox, because the input loads of these two gearbox are the same and certain gearbox components are necessary to withstand the input loads.

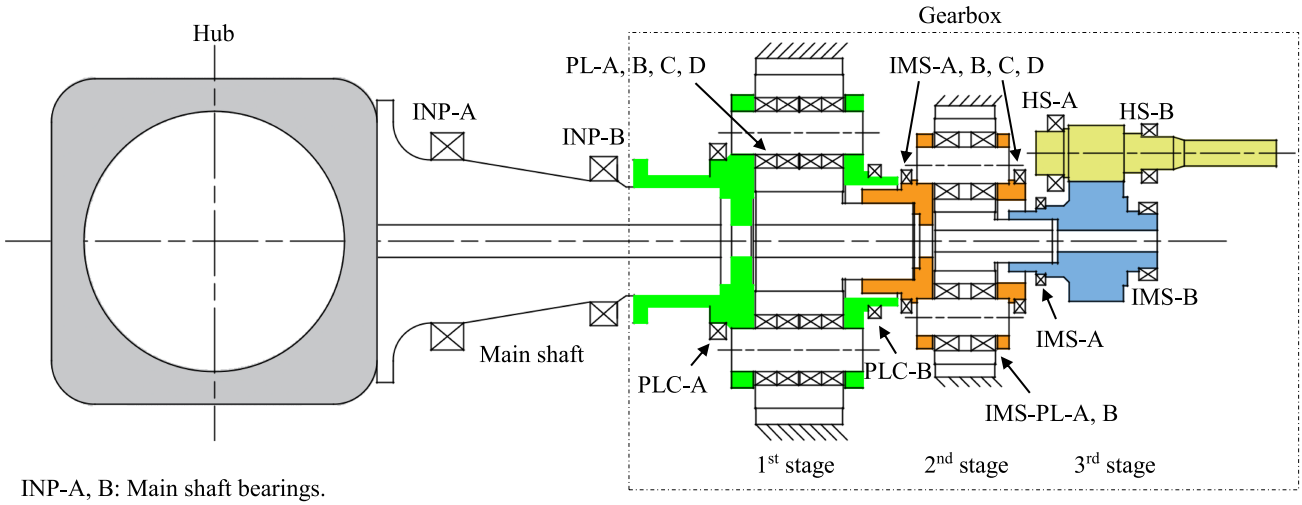

INP-A, B: Main shaft bearings.
PLC-A, B: Planet carrier bearing in the first stage; PL-A, B, C, D: Planet bearings in the first stage.
IMS-PLC-A, B: Planet carrier bearing in the second stage; IMS-PL-A, B: Planet bearings in the second stage.
IMS-A, B: Intermediate shaft bearings in the third stage; HS-A, B: High speed shaft bearings in the third stage.

(A) Conventional gearbox configuration[3]

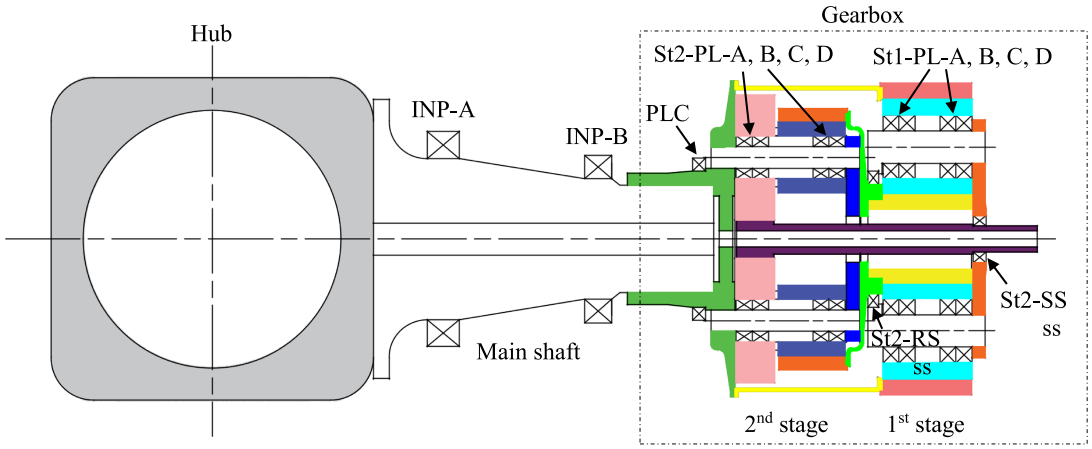

PLC: Planet carrier bearing.
St1-PL-A, B, C, D: Planet bearings in the first stage.
St2-PL-A, B, C, D: Planet bearings in the second stage.
St2-RS: Ring shaft bearing in the second stage.
St2-SS: Sun shaft bearings in the second stage.

(B) Compact gearbox configuration[6]

FIGURE 1 Conventional and compact gearbox configurations [Colour figure can be viewed at wileyonlinelibrary.com]

3 | METHODOLOGY

3.1 | Environmental conditions

In this study, the 10 MW wind turbine is supported on a monopile foundation at an offshore site in 30 m water depth. Five combined wind and wave conditions are selected to conduct the dynamic simulations of the 10 MW offshore wind turbine, as given in Table 2. All the environmental conditions are selected based on a long-term joint distribution obtained from 10 years' hindcast wind and wave data for a location in the Northern North Sea, which is described as site 15 in the study of Li et al.[17]

The five mean wind speeds at hub height (u) are selected to cover the whole operational range of the turbine, and the wave conditions correspond to the most probable significant wave height H_s and spectral peak period T_p for each mean wind speed. The 1 h mean wind speed at 10 m above the average sea level (u_{10}) follows a two-parameter Weibull distribution, and the probability density function $f_{U_{10}}(u_{10})$ is given by[17]

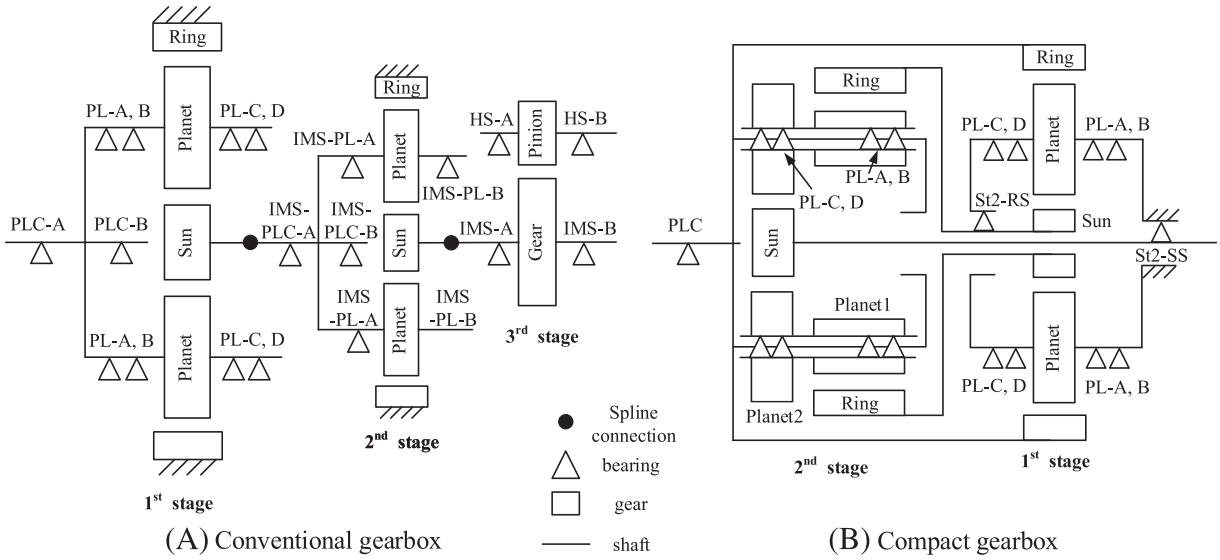

FIGURE 2 10 MW conventional and compact gearbox topologies[3,6]

TABLE 1 Ten MW conventional and compact gearbox specifications[6]

Parameter	Conventional	Compact
Gearbox type	Three stages	Two stages
First stage gear ratio	1:4.423	1:3.219
Second stage gear ratio	1:5.192	1:15.587
Third stage gear ratio	1:2.179	—
Total gear ratio	1:50.039	1:50.172
Power distribution by first stage	—	74.776%
Power distribution by second stage	—	25.224%
Designed power (kw)	10 000	Same
Rated input shaft speed (rpm)	9.6	Same
Generator shaft speed (rpm)	480.4	484.6
Total gearbox dry weight (×1000 kg)	60.43	57.41
Maximum gear outer diameter (m)	3.098	2.710
Gearbox length (m)	5.964	3.328
Service life (year)	20	Same

TABLE 2 Environmental conditions in the normal operational conditions

EC	EC1	EC2	EC3	EC4	EC5
u (m/s)	5	8	12	16	24
H_s (m)	0.8	1.2	1.9	2.7	4.6
T_p (s)	5.3	5.8	6.6	7.4	9

$$f_{U_{10}}(u_{10}) = \frac{\alpha_U}{\beta_U}\left(\frac{u_{10}}{\beta_U}\right)^{\alpha_U - 1} exp\left[-\left(\frac{u_{10}}{\beta_U}\right)^{\alpha_U}\right], \tag{1}$$

where α_U and β_U represent the shape and scale parameters of the Weibull distribution and they are 2.299 and 8.920, respectively.[17]

The mean wind speed at hub height is calculated based on a power law formulation:[18]

$$u = u_{10}\left(\frac{z_{hub}}{10}\right)^{\alpha}, \tag{2}$$

where u represents the mean wind speed at the hub height z_{hub} above the still water level; z_{hub} = 119 m for the 10 MW wind turbine. α denotes the power law exponent; α = 0.14 is used based on the IEC 61400-3.[18]

Based on Equations 1 and 2, the probability density function of the mean wind speed at hub height is obtained, which is presented in Figure 3 together with the selected five environmental conditions. Each simulation is carried out for 4000 s, and the first 400 s are removed to avoid start-up transient effects.

Three-dimensional tubulent wind files are generated by the NREL TurbSim program[19] according to the Kaimal turbulence model for Class B turbines that is defined in the IEC 61400-1.[20] The normal turbulence model and normal wind profile model are considered for all of the load cases. Wave series are generated using the JONSWAP spectrum with given H_s and T_p. All load cases consider wind and waves aligned in the positive wind direction. Current is not considered in this study.

3.2 | Computational gearbox model

The numerical models of the wind turbine gearboxes are established using the commercial package SIMPACK,[21] which is a multi-body system (MBS) software that has been widely used for wind turbine drivetrain dynamic analysis.[22-24] Since the gearbox is one part of drivetrain system, its dynamics will be affected by other components. Hence, in order to accurately describe the dynamic behaviour of the gearbox, the hub, main shaft, main bearings, torque arms, housing, generator and bedplate are considered. These components, which are identical in the two numerical models, were designed for the conventional gearbox. A detailed description of the drivetrain model can be found in the study of Wang et al.[3] The 10 MW drivetrain numerical models used in this study are presented in Figure 4.

Based on the recommendations from Guo et al.[25] on model fidelity for wind turbine gearbox dynamic simulation, the main shaft, planet carriers and shafts inside the gearbox are modelled with reduced finite element (FE) bodies. The FE bodies are established in ANSYS and are reduced using the Craig-Bampton modal reduction technique.[26] Hub, housing, bedplate, gears and planet pin shafts are treated as rigid bodies. Gear tooth contact is modelled by a specific force element, FE225, in SIMPACK. Gear contact forces are composed of the stiffness force, the damping force and the friction force. The gear tooth stiffness is calculated in accordance with international standard ISO 6336-1.[27] Bearings are modelled using linear diagonal stiffness matrices, which is described in the previous study.[3] Since tapered roller bearing (TRB) mounting usually requires preloaded operation, the bearing clearance of this type of bearing is not considered, while it is considered for cylindrical roller bearings (CRBs) and the clearance values are taken from a bearing manufacturer's catalogue.

A two-step decoupled analysis method, which has been effectively used in earlier studies,[28-30] is employed for the gearbox load effect analysis. First, global aero-hydro-servo-elastic analysis of the wind turbine with a simplified drivetrain, which is modelled by a single degree-of-freedom (DOF) torsional spring-damper system, is conducted in SIMA.[31] Then, the loads and motions obtained from the global simulations are used as the input to the gearbox dynamic response analysis. More specifically, forces and bending moments are extracted from the tower top, and then they are transformed to the hub centre via load-balance relationships among components in the nacelle system. Additionally, nacelle displacements, velocities and accelerations are applied at the bottom of the bedplate in the computational drivetrain models. To maintain the correct generator speed, generator feedback torque is applied on the generator shaft based on a proportional-integral (PI) velocity controller, which is described in detail in the studies of Xing et al.[32,33] In the present study, all the gearbox local response results are based on the coordinate system shown in Figure 4.

3.3 | Dynamic load-sharing factor calculation

Gearbox load-sharing performance directly reflects the smoothness and reliability of the wind turbine transmission system. Ideally, the loads on each planet transmission path should be equal, but inevitable factors, such as manufacturing and installation errors, elastic deformation of

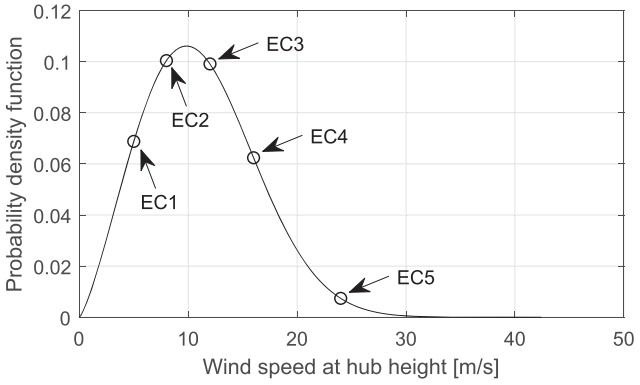

FIGURE 3 Probability density function of mean wind speed at wind turbine hub height

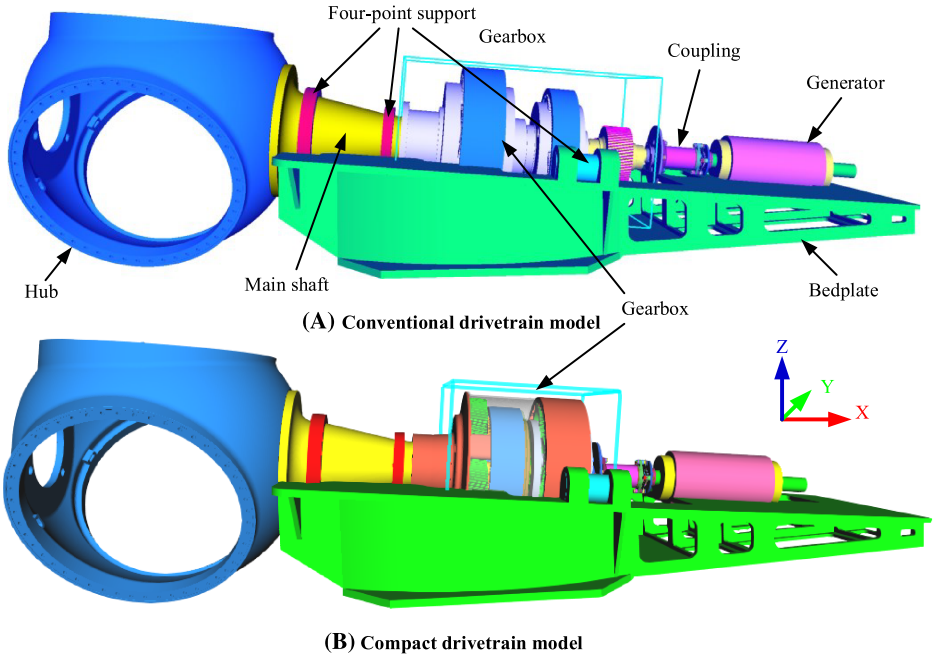

FIGURE 4 Ten MW conventional and compact drivetrain dynamic models [Colour figure can be viewed at wileyonlinelibrary.com]

components and external non-torque loads, result in unevenly distributed loads across multiple paths. This uneven transmission significantly affects the lifetime of the wind turbine gearbox. According to the American Gear Manufacturers Association (AGMA) 6123-B06[34] for enclosed epicyclic gear drives, the load-sharing factor K_γ is the ratio between the maximum and average planet transmitted loads:[34]

$$K_\gamma(t) = \frac{max(F_{pi}(t))}{\frac{1}{n}\cdot\sum_{i=1}^{n}(F_{pi}(t))}, \tag{3}$$

where $K_\gamma(t)$ is the dynamic load-sharing factor, i denotes the planet number, n represents the number of planets, and $F_{pi}(t)$ is the dynamic meshing force between Sun-planet gear pairs or ring-planet gear pairs. The load-sharing factor K_γ varies in time. In this study, the maximum value and mean value of K_γ over time are used for the comparative analysis between the conventional and compact gearboxes.

3.4 | Fatigue damage calculation

3.4.1 | Gear fatigue damage calculation

In this study, 1 h gear tooth contact and bending fatigue damage are calculated based on the Palmgren-Miner linear accumulative damage hypothesis:[35]

$$D(u,H_s,T_p) = \sum_i \frac{n_i(u,H_s,T_p)}{N_i(u,H_s,T_p)} = \frac{1}{k}\sum_i n_i(u,H_s,T_p)\cdot s_i(u,H_s,T_p)^m, \tag{4}$$

where u, H_s and T_p represent the mean wind speed at hub height and corresponding significant wave height and spectral peak period, respectively. $D(u, H_s, T_p)$ is the 1 h accumulated gear tooth fatigue damage under the environmental condition u, H_s, T_p. $s_i(u, H_s, T_p)$ is the gear tooth stress range, which is obtained using the LDD method. A detailed description of the method can be found in the study of Wang et al.[36] $N_i(u, H_s, T_p)$ is the permissible number of cycles under gear tooth stress range $s_i(u, H_s, T_p)$ and is calculated according to the gear SN-curve given as $N_i(u,H_s,T_p) = k\cdot s_i(u,H_s,T_p)^{-m}$, where k and m are SN-curve parameters that depend on factors such as the gear material, heat treatment method and processing method. In this study, the ring gears in the two gearboxes are assumed to be made of 42CrMo4, and they are processed by induction hardening. Moreover, Sun gears and planet gears are assumed to be made of 18CrNiMo7-6, and they are processed by carburizing. The material strength of all the gears corresponds to the MQ quality in ISO 6336-5.[12] The SN-curve parameters k and m are calculated based on ISO 6336-2[13] and ISO 6336-3,[14] respectively.

The number of stress cycles n_i under the stress bin i is found as[37]

$$n_i = \sum_j \frac{t_j w_j}{2\pi}, \tag{5}$$

where t_j is the jth time duration of the stress bin i. w_j is average gear rotational speed (rad/s) in jth time duration of the stress bin i.

3.4.2 | Bearing fatigue damage calculation

The 1 h bearing fatigue damage is calculated based on the linear damage accumulation law:

$$D(u, H_s, T_p) = \sum_i \frac{l_i(u, H_s, T_p)}{L_{10i}} = \frac{1}{c^a} \sum_i l_i(u, H_s, T_p) \cdot p_i^a, \tag{6}$$

where u, H_s and T_p represent the mean wind speed at hub height and corresponding significant wave height and wave peak period, respectively. $D(u, H_s, T_p)$ is the 1 h accumulated bearing fatigue damage under the environmental condition u, H_s, T_p. p_i is the bearing equivalent load range, which is obtained via a two-step process. First, the bearing equivalent load P is calculated as $P = XF_r + YF_a$, where F_r and F_a are bearing radial and axial loads, respectively, obtained from the dynamic simulation and X and Y are dynamic loading factors from the bearing standard ISO 281.[16] Next, p_i is obtained via the LDD method. l_i is the number of bearing load cycles under the load range p_i, which is calculated based on Equation 5. L_{10i} is the bearing life to failure under the load range p_i, which is estimated based on the load-life relationship:[16]

$$L_{10} = \left(\frac{C}{P}\right)^a, \tag{7}$$

where L_{10} is the basic rated life (10^6 revolutions (r)). L_{10} is defined as the number of cycles when fatigue damage appears in 10% of bearings, while the other 90% of bearings work normally in one test. C is the basic dynamic load rating, which is a specific constant for a given bearing. a is the bearing life factor: for ball bearings, $a = 3$, and for roller bearings, $a = \frac{10}{3}$.

4 | RESULTS AND DISCUSSIONS

4.1 | Comparisons of gearbox dynamic behaviour under pure torque load cases

In this section, comparisons of the dynamic behaviour of the two gearboxes under pure torque load cases (LCs) are presented. Figure 5 shows 1 h time series of torque under five load cases that are used as the input to the dynamic analysis of the conventional and compact gearboxes. The five load cases correspond to the five environmental conditions presented in Table 2. The wind turbine reaches the rated operational condition from LC3, while LC1 and LC2 are below the rated condition.

Figure 6 compares the maximum value and the mean value of $K_\gamma(t)$ between the conventional and the compact gearboxes under all load cases. Since the second stage in the compact gearbox adopts a compound epicyclic planet gear set, both the Sun-planet gear set and ring-planet gear set are analysed, as shown in Figure 6B. In both the first and second stages, the maximum and the mean values of $K_\gamma(t)$ of the conventional gearbox are higher than those of the compact gearbox under all load cases.

To understand the results for $K_\gamma(t)$, the motion responses of floating components in the two gearboxes are studied. Figure 7 shows the motion orbits of the floating Sun and ring gears in the conventional and compact gearboxes under LC3. In the first stage, the Sun gear motion orbit in the

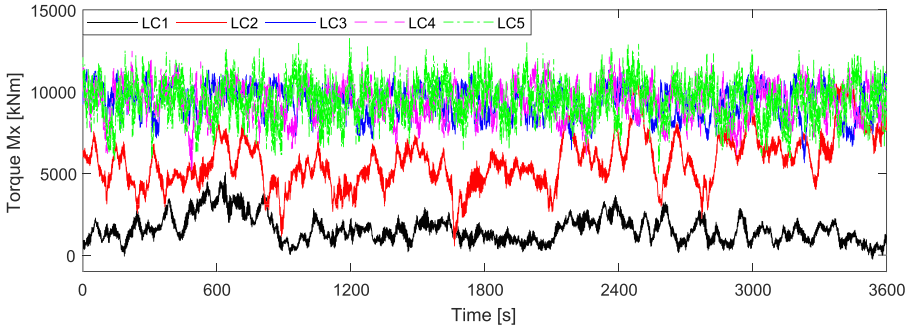

FIGURE 5 One hour time series of torque under five load cases [Colour figure can be viewed at wileyonlinelibrary.com]

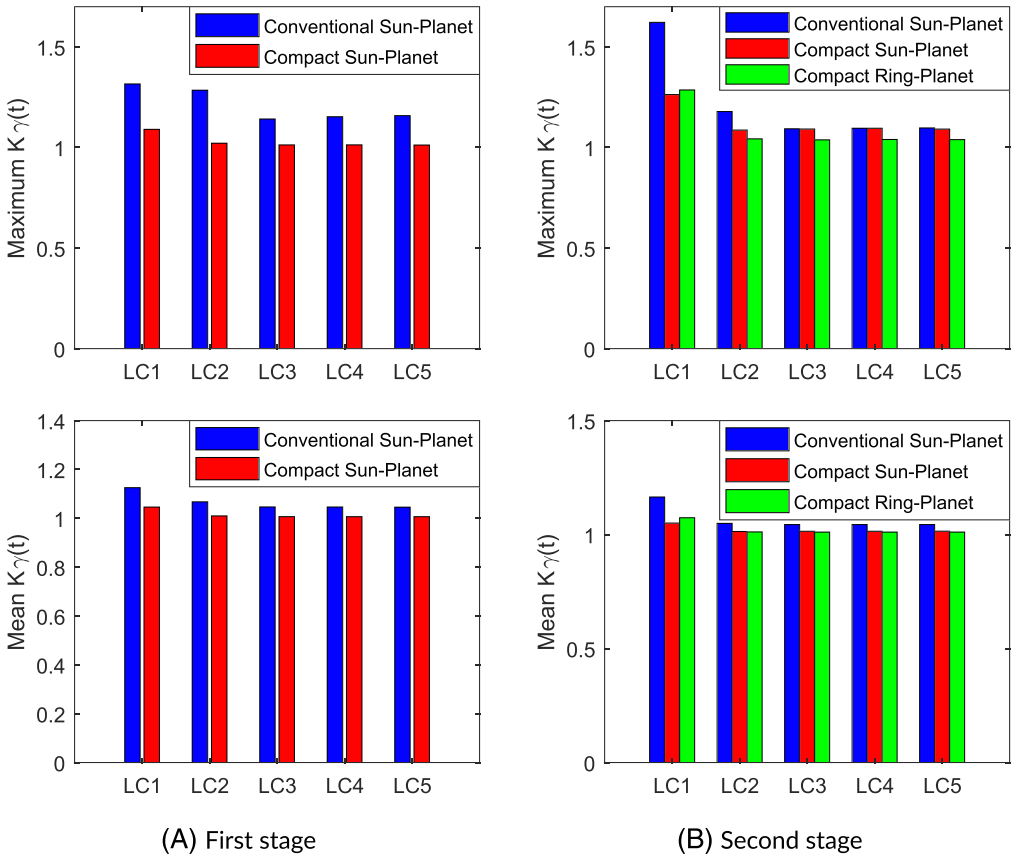

FIGURE 6 Comparison of maximum and mean values of dynamic load-sharing factors between conventional and compact gearboxes under all load cases [Colour figure can be viewed at wileyonlinelibrary.com]

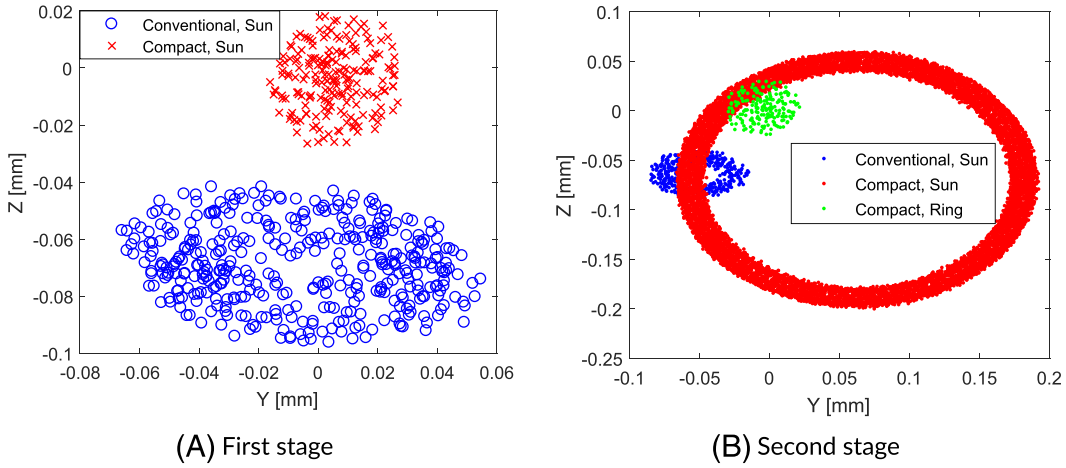

FIGURE 7 Comparison of floating Sun (ring) gear motion orbit between conventional and compact gearboxes under load case LC3 [Colour figure can be viewed at wileyonlinelibrary.com]

conventional gearbox deviates significantly from the centre position in the gravity (*Z*) direction. This is because a CRB bearing is used for the downwind planet carrier bearing PLC-B in the conventional gearbox and a 0.535 mm bearing radial internal clearance is considered. The Sun gear motion orbit therefore moves down due to gravitational effects from the planet carrier, planet gears and bearings as well as the Sun shaft. These gravitational effects can be illustrated by the FFT spectrum analysis for the Sun-planet meshing force of the two gearboxes, as shown in Figure 8. In the first stage, the Sun-planet meshing force spectrum of the conventional gearbox is dominated by the input shaft rotational frequency response, which is mainly caused by the gravity of the first planetary stage components. In contrast, the Sun gear in the compact gearbox has a good motion orbit, as shown in Figure 7A, because the first stage planet carrier is fixed and the planet carrier gravitational forces will affect the

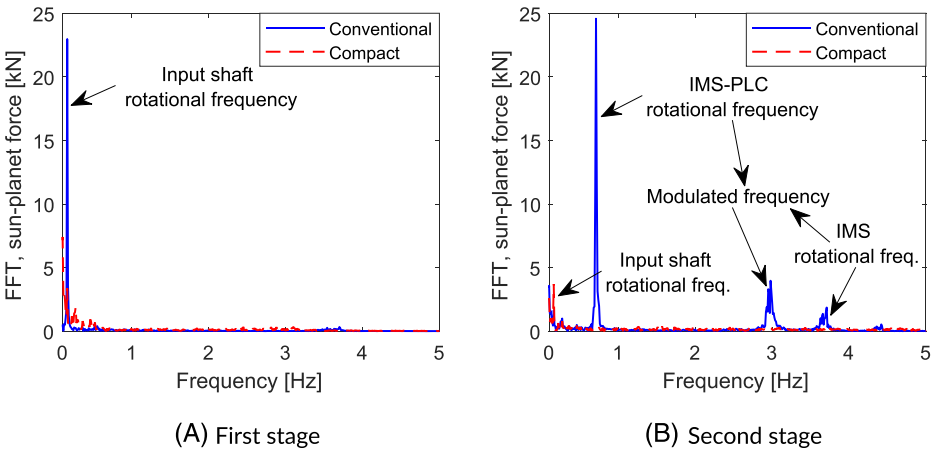

FIGURE 8 Comparison of FFT of the Sun-planet meshing force between conventional and compact gearboxes under load case LC3 [Colour figure can be viewed at wileyonlinelibrary.com]

Sun gear motion. No significant low-frequency response is visible in the Sun-planet meshing force in the compact gearbox. Although the conventional gearbox Sun gear floats more than the Sun gear in the compact gearbox, the load distribution among planet gears in the conventional gearbox is still more uneven than that of the compact gearbox, which implies that the floating capacity of the Sun gear is not sufficient to offset the uneven load-sharing among planet gears caused by gravity.

In the second stage, the motion orbit of the Sun gear in the compact gearbox is significantly larger than that of the Sun gear in the conventional gearbox. The ring gear in the compact gearbox has a good motion orbit; namely, it has a small amount of floating and is in the centre position, as shown in Figure 7B. The large floating of the Sun gear in the compact gearbox is primarily due to its large floating capacity, since the Sun shaft in this stage is designed to be long, as shown in Figures 1B and 2B. Additionally, the Sun gear motion orbits in both the conventional and compact gearboxes are out of the centre position, which primarily due to gravity effects. However, the large amount of floating of the Sun gear in the compact gearbox significantly mitigates the gravity effects; in contrast, due to the limited floating capacity of the Sun gear in the conventional gearbox, the gravity effects on the load-sharing are still prominent. This can be seen in the frequency analysis for the Sun-planet meshing force, as shown in Figure 8B. In the amplitude spectrum associated with the conventional gearbox, peaks primarily appear at the intermediate planet carrier rotational frequency, the intermediate shaft rotational frequency and their modulation frequency, which implies that the load-sharing among planet gears is certainly affected by the gravity of the intermediate planetary stage components. Although the input shaft rotational frequency appears in the amplitude spectrum associated with the compact gearbox, the gravity effects on the gear meshing force are apparently slight.

4.2 | Comparisons of gearbox dynamic behaviour under tangential pin position error conditions

In practice, manufacturing and assemble errors on planetary gears are inevitable. Tangential pin position error is a common manufacturing tolerance type that significantly affects planetary load sharing.[38,39] In this section, the dynamic responses of the two gear boxes under tangential pin position error conditions are compared. More specifically, five tangential pin error cases increasing from 0.1 to 0.5 mm are defined, which are applied on planet 1 (the first planet which is located at the top position in the gravity direction) in both the first stage and the second stage of the conventional and compact gearboxes. The magnitudes of the tangential pin error considered in the 10 MW gearboxes are inferred based on the measured values for smaller gearboxes, as demonstrated in the studies of Austin[40] and Park et al.[41] Error sensitivity analysis is conducted for both gearboxes. Based on this analysis, the dynamic behaviour of the two gearboxes is assessed and compared. Dynamic simulations for cases of applying pin position errors on the first stage planet are conducted separately from those on the second stage planet, which implies that when the pin position errors are applied on one stage, the other stage does not consider any errors. Note that the comparative analysis is only conducted under rated torque load case LC3, which is the load case which represents the largest duration within the wind turbine life cycle.

4.2.1 | Load-sharing behaviour comparison

Figure 9 presents the time series of the planet load sharing in the first stage of the conventional and the compact gearbox under 0.3 mm pinhole position error. Planet 1 in both gearboxes carries a larger portion of the load than other planets because the tangential pin position error causes it to come into contact earlier than other planets. Additionally, the fluctuating characteristics of the planet gear teeth loads over time are different in these two gearboxes. An apparent cyclical fluctuation can be seen in the time series of the planet gear teeth loads of the conventional gearbox because the planet carrier in this stage is rotational, while the cyclical fluctuation does not appear in the compact gearbox since its planet carrier is fixed.

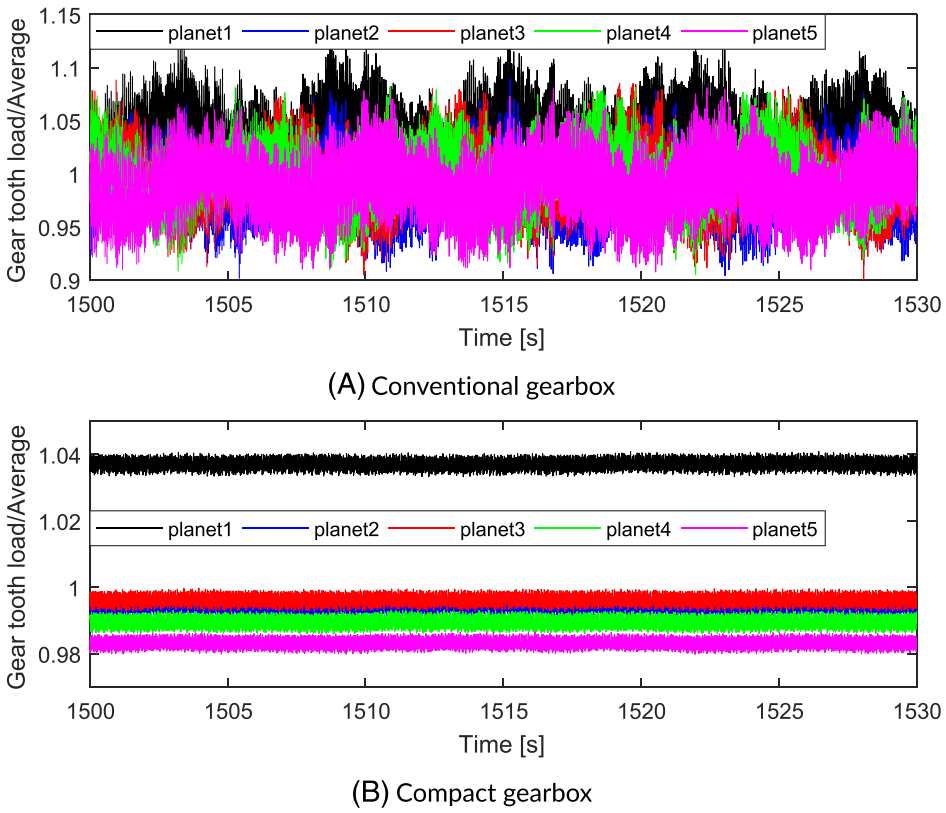

FIGURE 9 Sun-planet load sharing in the first stage of the conventional and compact gearboxes under 0.3 mm pinhole position error condition under load case LC3 [Colour figure can be viewed at wileyonlinelibrary.com]

Figure 10 compares the maximum and the mean values of dynamic load-sharing factors between the conventional and the compact gearbox under all defined tangential pin position error conditions. Under all error conditions, both the maximum and the mean values of the dynamic load-sharing factors of the conventional gearbox are larger than those of the compact gearbox, in both the first stage and second stage. The reasons are attributed to the conclusions in section 4.1: In the first stage, the relatively poor load-sharing performance of the conventional gearbox is due to the component gravity effects, while in the second stage, it is due to the relatively small sun gear floating capacity. Additionally, in the second stage, both the maximum and mean values of $K_\gamma(t)$ in the conventional gearbox increase sharply as the pin position error increases, while the compact gearbox load sharing is almost invariable with the increasing error. The load-sharing performance of the conventional gearbox is thus more sensitive to the tangential pin position error than the compact gearbox.

To understand the differences in sensitivity, the motions of the floating components in these two gearboxes under all error conditions are studied. Time series of the Sun gear *Y* motion in the first stage of the two gearboxes, in Figure 11, is used as an example. The amplitude of the Sun gear motion in the conventional gearbox increases at a once-per-carrier revolution as the error increases, while its mean values do not change significantly. In contrast, the variation of the Sun gear motion in the compact gearbox mainly appears in the mean values. This is because the planet carrier design differs in these two gearboxes: A rotational design is adopted in the conventional gearbox, and a fixed design is used in the compact gearbox. The unevenly shared planet gear loads in the conventional gearbox vary cyclically along with the carrier revolution, while the planet carrier of the compact gearbox is fixed. This difference also explains the characteristics of Figure 12, where the error sensitivities of the floating component radial motion in the first stage are compared. Generally, in the first stage, the mean values of *Y* and *Z* motion in the conventional gearbox are invariable with the increases of tangential pin position error, while dramatic increases appear in their standard deviations. For the compact gearbox, an approximately linear relationship is seen between the pin position error and the mean value of Sun gear motion, while the standard deviations of sun gear motions are invariable.

Figure 13 compares the error sensitivities for floating component radial motion in the second stage between these two gearboxes. Since the second stages in both these two gearboxes adopt a rotational planet carrier design, the mean values of Sun gear motion vary only slightly with increasing error, and the main increases are seen in their standard deviations. One exception is the ring gear motion in the compact gearbox that has poor floating capacity due to a close bearing support. The standard deviations of Sun gear motions in the compact gearbox are slightly more sensitive to the error magnitude than in the conventional gearbox, but the main reason for the stable load-sharing behaviour is the large amount of floating of the Sun gear in the compact gearbox. In contrast, although the amplitude of the Sun gear motion in the conventional gearbox increases significantly as the error magnitude increases, it still cannot alleviate the increase in the unevenness of the load sharing caused by the increased error.

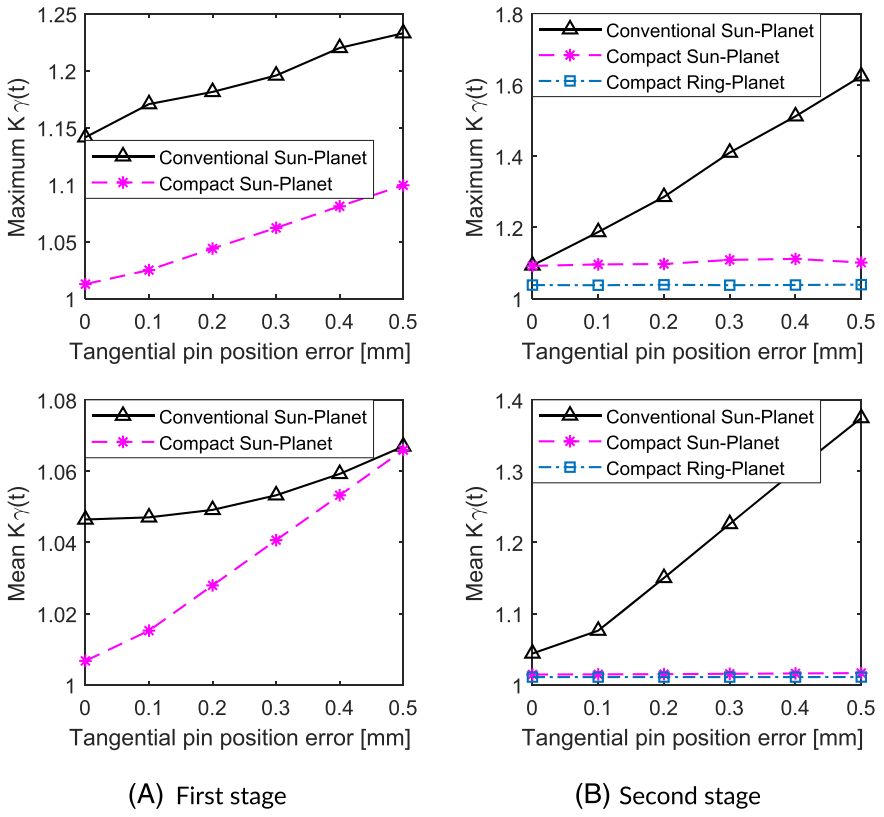

FIGURE 10 Comparison of maximum and mean values of dynamic load-sharing factors between conventional and compact gearboxes under tangential pin position error conditions [Colour figure can be viewed at wileyonlinelibrary.com]

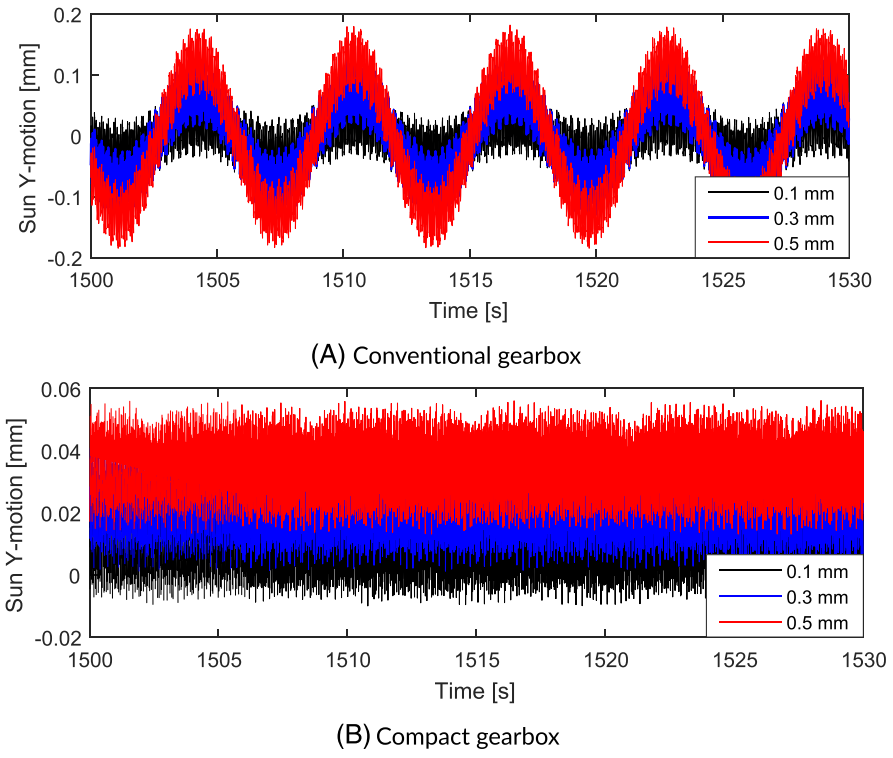

FIGURE 11 Sun-planet load sharing in the first stage of the conventional and compact gearboxes under 0.1, 0.3 and 0.5 mm tangential pinhole position error conditions [Colour figure can be viewed at wileyonlinelibrary.com]

4.2.2 | Relative fatigue damage comparison

In this section, the sensitivity of fatigue damage of gears and bearings to tangential pin position error is compared between the conventional gearbox and the compact gearbox. This is expressed by relative damage, defined as

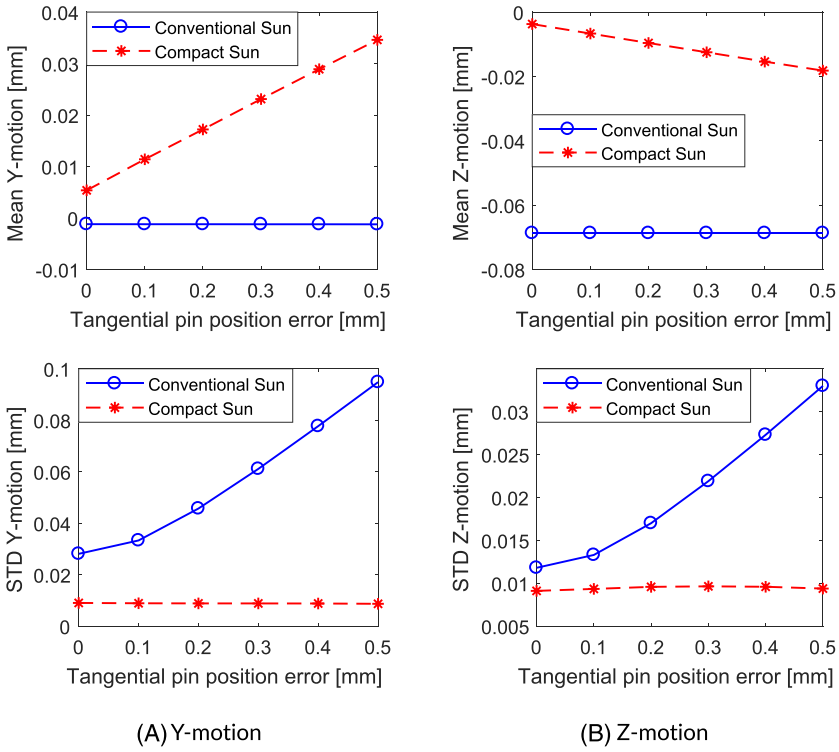

FIGURE 12 Comparison of error sensitivities on Sun gear radial motion in the first planetary stage of conventional and compact gearboxes; (a) mean value and standard deviation of *Y* motion; (b) mean value and standard deviation of *Z* motion [Colour figure can be viewed at wileyonlinelibrary.com]

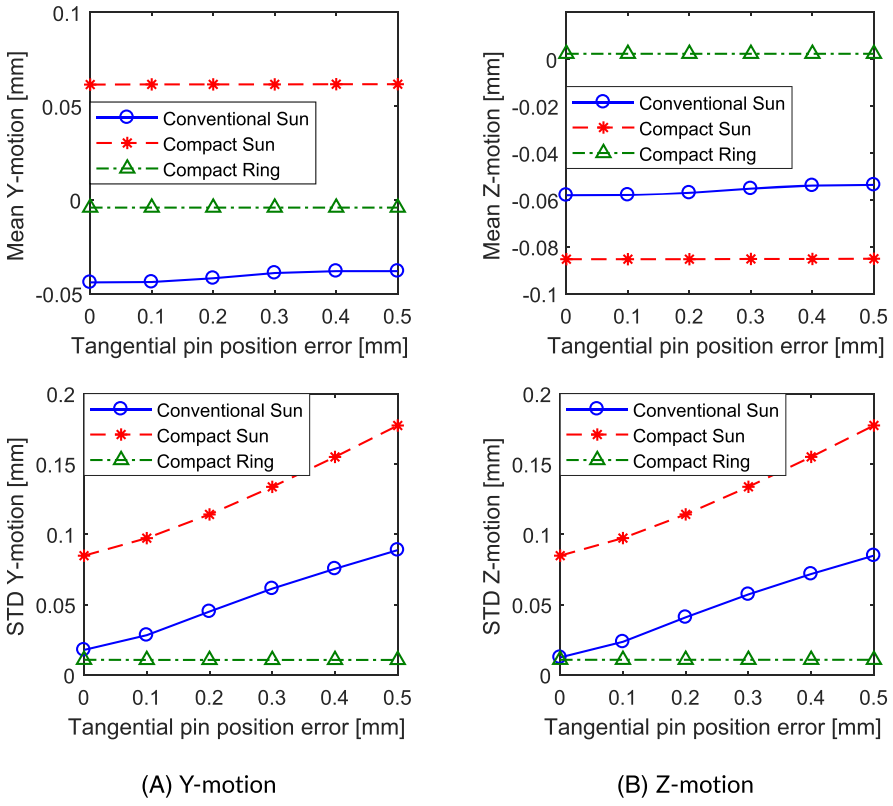

FIGURE 13 Comparison of error sensitivities on Sun (ring) gear radial motion in the second planetary stage of conventional and compact gearboxes; (a) mean value and standard deviation of *Y* motion; (b) mean value and standard deviation of *Z* motion [Colour figure can be viewed at wileyonlinelibrary.com]

$$relative\ damage = \frac{D_{with\ error}}{D_{without\ error}}, \tag{8}$$

where $D_{with\ error}$ and $D_{without\ error}$ are the 1 h fatigue damage of gears and bearings with and without error conditions in these two gearboxes, respectively.

Table 3 compares the relative damage of components between these two gearboxes under all error cases. A high relative value implies the component fatigue damage is very sensitive to the given pin position error.

The fatigue damage of a total of 11 components will be affected in the conventional gearbox under tangential pin position error conditions, while only four components will be affected in the compact gearbox. This implies that the conventional gearbox is more susceptible to fatigue damage related to manufacturing errors. Generally, the number of affected components of the conventional gearbox, which are marked with colors, increases with the error increases.

The increase in fatigue damage of the compact gearbox remains below 50% for pin position errors below 0.5 m, while smaller errors result in larger damage increases for the conventional gearbox. Moreover, in the 0.5 mm error condition, the fatigue damage of five components are obviously affected in the conventional gearbox. For the planet gear in the second stage, more than tenfold increases in bending and pitting fatigue damage are observed. These results generally suggest that the fatigue damage of the conventional gearbox is more sensitive than the compact gearbox to pin position errors.

4.3 | Comparisons of gearbox dynamic behaviour under non-torque loads

In this section, the effects of non-torque loads on the conventional gearbox and the compact gearbox are compared. This is also expressed by relative damage, defined as

$$relative\ damage = \frac{D_{with\ non-torque\ load}}{D_{without\ non-torque\ load}}, \tag{9}$$

where $D_{with\ non-torque\ load}$ and $D_{without\ non-torque\ load}$ are the 1 h fatigue damage of gears and bearings under with and without non-torque load cases in these two gearboxes, respectively. It is noted that the pin position error is no longer considered in this section.

TABLE 3 Conventional versus compact gearbox

		Tangential pin position error (mm)				
Gearbox	**Components**	**0.1**	**0.2**	**0.3**	**0.4**	**0.5**
Conventional	PLC-A	1.02	1.10	1.21	1.38	1.60
	PL-A	1.04	1.08	1.12	1.17	1.21
	IMS-PLC-A	1.11	1.44	1.98	2.70	3.57
	IMS-PLC-B	1.03	1.09	1.18	1.26	1.36
	IMS-PL-A	1.26	1.58	1.96	2.44	3.01
	IMS-A	1.16	1.56	2.11	2.81	3.69
	IMS-B	1.04	1.17	1.36	1.57	1.79
	St1-Sun-bending	1.01	1.02	1.03	1.04	1.06
	St1-planet-bending	1.08	1.17	1.27	1.37	1.48
	St2-Sun-bending	1.06	1.26	1.67	2.39	3.56
	St2-planet-bending	1.64	2.64	4.23	6.76	10.70
	St1-Sun-pitting	1.01	1.02	1.03	1.05	1.06
	St1-planet-pitting	1.09	1.18	1.29	1.40	1.51
	St2-Sun-pitting	1.07	1.30	1.77	2.63	4.05
	St2-planet-pitting	1.67	2.75	4.47	7.28	11.70
Compact	St1-PL-A	1.04	1.08	1.13	1.17	1.22
	St2-RS	1.05	1.09	1.15	1.20	1.26
	St1-Sun-bending	1.02	1.07	1.08	1.09	1.10
	St1-planet-bending	1.15	1.24	1.35	1.46	1.58
	St1-Sun-pitting	1.00	1.01	1.02	1.04	1.05
	St1-planet-pitting	1.16	1.26	1.37	1.49	1.62

Note. Comparison of relative fatigue damage (with error/without error). Green value (1.5–2.0): low relative damage; yellow value (2.0–6.0): medium relative damage; red value (>6.0): high relative damage.

The drivetrain design adopts a two-main-bearing support configuration to protect the gearbox from non-torque load effects, but certain bending moments enter the gearbox nonetheless due to the deflections of bedplate and gearbox housing as well as the tolerances in the assembly.[42] Additionally, a certain amount of the thrust force will also be inevitably transmitted into the gearbox due to main bearing clearance. The amount that is transmitted depends on the arrangement, clearances and axial stiffness of main bearings. In this study, the sensitivity of the gearbox dynamics to the pitching moment (M_y) and the thrust force (F_x) is examined. Both the pitch moment and thrust force are considered via five load cases: 2%, 4%, 6%, 8% and 10% of the loads that are obtained from the global analysis under the environmental condition EC3. The non-torque loads are applied at the main shaft-planet carrier connection position to ensure that the non-torque load transmitted into the gearbox is the designated one.

4.3.1 | Pitching moment load sensitivity analysis

In this section, the effects of a pitching moment on dynamic behaviour of the two gearboxes are studied. In addition, the sensitivity of fatigue damage to the pitch moment between the two gearboxes are compared. Figure 14 presents the time series of pitch moment under the five load cases. Figures 15–17 and 18–20 compare the gear meshing force and bearing radial (*Z* direction) force in time and frequency domain between the 10% M_y case and base case (M_y) in the conventional and the compact gearbox, respectively.

The 3P, 6P and 9P frequencies dominate the frequency content of the pitching moment spectra. The responses at these frequencies in the spectra of Figures 15–20 indicate that the gearbox load effects are affected by the pitching moments. In the conventional gearbox, 3P, 6P and 9P responses dominate in the spectra of planet bearing (PLC-A and PLC-B) load. The 1P response dominates in the spectrum of the Sun-planet meshing force, and the response value under the 10% M_y case is higher than the base case. This implies that the majority of bending moments are carried by the planet carrier bearings; the bending moments are not be transmitted directly to the gears but will exaggerate the planet carrier gravity effects on gear meshing.

In contrast, in the compact gearbox, in addition to the significant effects on the planet carrier bearing PLC, apparent effects caused by bending moments appear in the Sun-planet meshing force in the first stage. The bearing PLC is supported on the left side, and no support is placed on the right side. The support arrangement is similar to a cantilevered beam, which results in the bending moment effects on the first stage gear meshing force. An interesting observation is found in the St2-RS force, as illustrated in Figure 20. Not only the 3P, 6P and 9P but also the 1P and the 2P responses are important in the St2-RS load spectrum under the 10% M_y load case. This is because the bearing St2-RS is placed in the middle of the first stage and the second stage in the compact gearbox, as illustrated in Figures 1b and 2b, and the bearing will be affected by loads from two stages. The 3P, 6P and 9P responses are induced by the first stage due to the input bending moment effects, while the 1P and the 2P responses are induced by the second stage due to gravity effects.

Table 4 compares the relative damage of gears and bearings between the conventional and the compact gearboxes under all pitch moment load cases. In the conventional gearbox, the fatigue damage of a total of seven components is affected by the applied pitch moments, while only five components are affected in the compact gearbox. In the conventional gearbox, both the upwind and the downwind planet carrier bearings in the first stage, PLC-A and PLC-B, as well as the upwind planet carrier bearing in the second stage, IMS-PLC-A, are found to be significantly affected by the applied pitch moments. The relative damage of PLC-B remains approximately constant under low pitch moment load cases, while it increases quickly from the 6% M_y load case. This is because the PLC-B adopts a CRB with clearance and the clearance is largely reduced under the high pitch moment load cases.

Another observation is that fatigue damage of the Sun gear, planet gear and planet bearings in the conventional gearbox is not sensitive to the applied pitch moments. This is because that mean values of the load effect of these components are not obviously affected by the pith moments. On the other hand, in the compact gearbox, fatigue damage effects are only observed in the planet carrier bearing PLC under high pitch moment cases. This is because the applied pitch moments are shared by the gears in the first stage. However, other

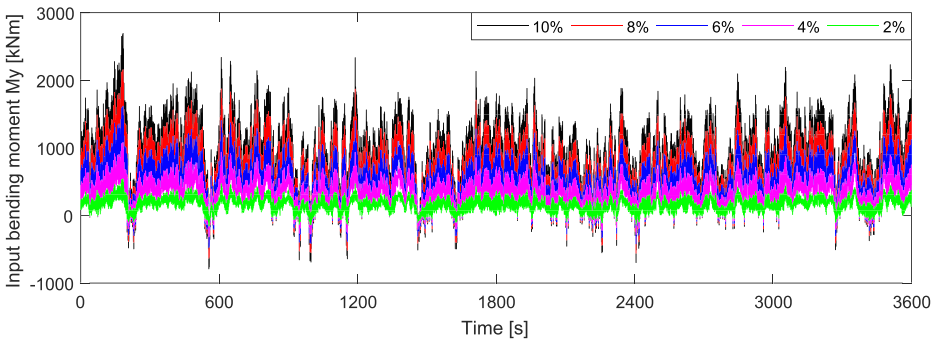

FIGURE 14 One hour time series of bending moment under five load cases [Colour figure can be viewed at wileyonlinelibrary.com]

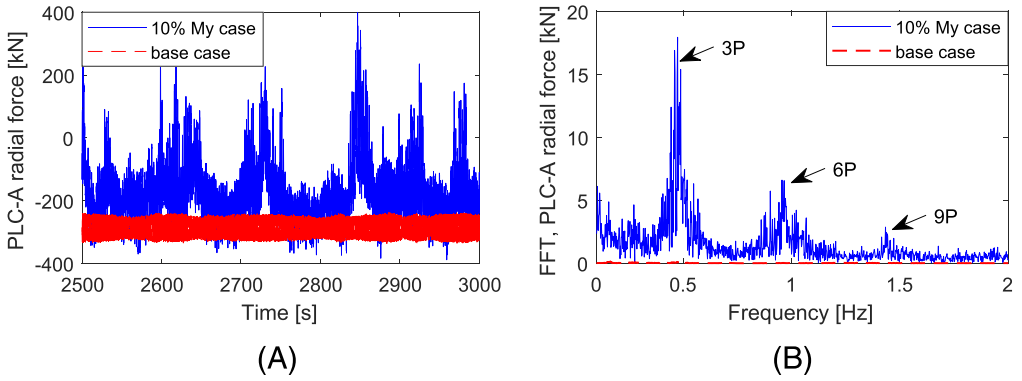

FIGURE 15 Comparison of time series and FFT of the PLC-A radial force between 10% M_y case and base case in the conventional gearbox [Colour figure can be viewed at wileyonlinelibrary.com]

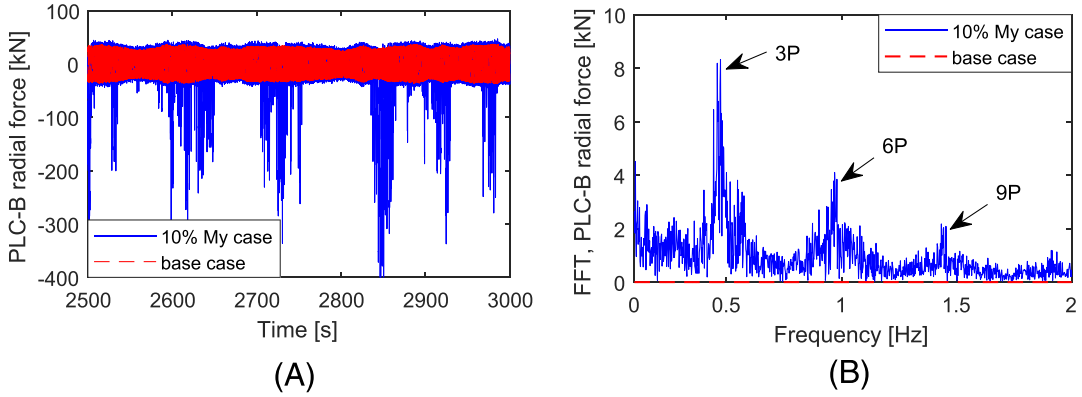

FIGURE 16 Comparison of time series and FFT of the PLC-B radial force between 10% M_y case and base case in the conventional gearbox [Colour figure can be viewed at wileyonlinelibrary.com]

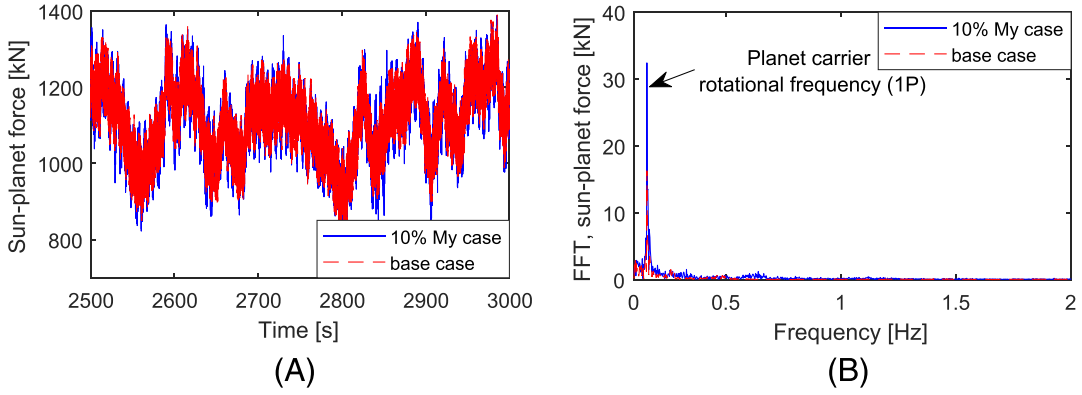

FIGURE 17 Comparison of time series and FFT of the Sun-planet meshing force between 10% M_y case and base case in the first stage of the conventional gearbox [Colour figure can be viewed at wileyonlinelibrary.com]

components in the compact gearbox are more sensitive to pitch moment than those in the conventional gearbox. This is because the planet carrier of the first stage of the compact gearbox is fixed and thus the pitch moment affects the mean values of gear and bearing load effects. The relative damage of PLC-A in the conventional gearbox and the PLC in the compact gearbox decrease with the increases of the applied bending moment M_y. This is because the clockwise pitch moments are applied at the planet carriers, mitigating the gravity effects of the planet carrier on these two bearings.

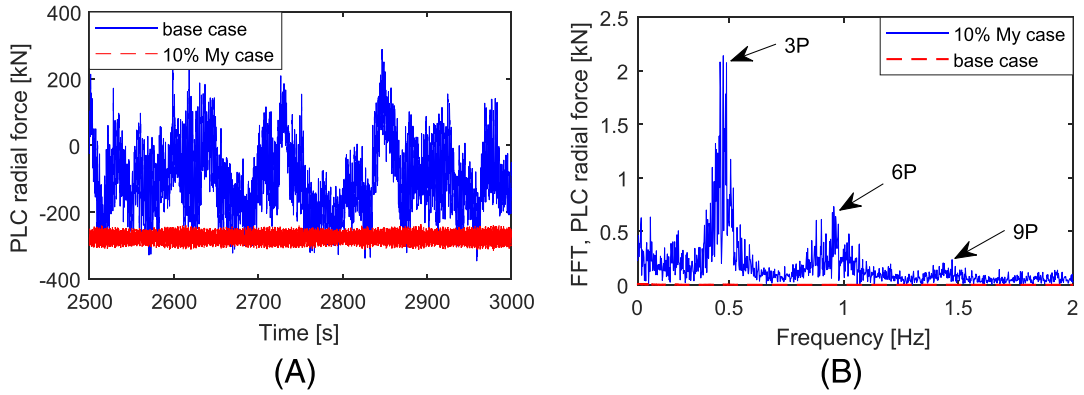

FIGURE 18 Comparison of time series and FFT of the PLC radial force between 10% M_y case and base case in the compact gearbox [Colour figure can be viewed at wileyonlinelibrary.com]

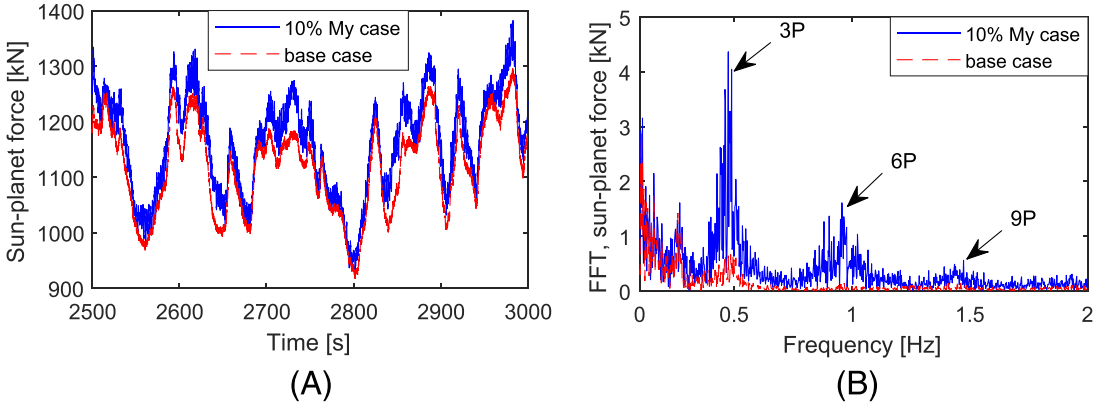

FIGURE 19 Comparison of time series and FFT of the Sun-planet meshing force between 10% M_y case and base case in the first stage of the compact gearbox [Colour figure can be viewed at wileyonlinelibrary.com]

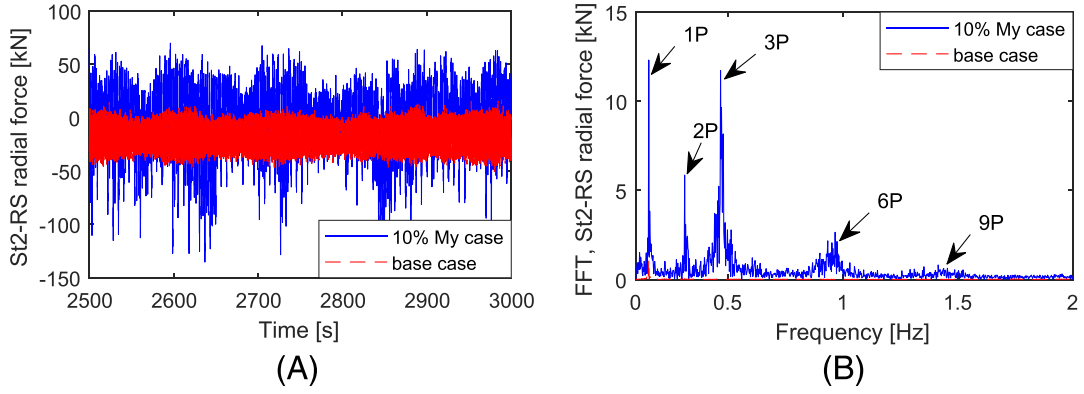

FIGURE 20 Comparison of time series and FFT of the St2-RS radial force between 10% M_y case and base case in the compact gearbox [Colour figure can be viewed at wileyonlinelibrary.com]

4.3.2 | Thrust force sensitivity analysis

In this section, the effect of the thrust force on load effects and fatigue damage of the most vulnerable component in these two gearboxes is conducted. Figure 21 presents the time series of thrust force under the five load cases. In these two gearboxes, one bearing designation, LL889049/LL889010D, is used in the same position, which corresponds to the PLC-A in the conventional gearbox and the PLC in the compact gearbox, as presented in Figure 1. However, the dynamic responses of these two bearings are different under all load cases.

TABLE 4 Conventional versus compact gearbox

Gearbox	Components	Bending moment M_y (kNm)				
		2%	4%	6%	8%	10%
Conventional	PLC-A	0.92	0.70	0.54	0.43	0.35
	PLC-B	1.80	1.80	1.92	3.82	11.06
	PL-A	1.00	1.00	1.00	1.00	1.00
	IMS-PLC-A	1.08	1.21	1.36	1.52	1.67
	IMS-PLC-B	1.02	1.03	1.03	1.04	1.05
	St1-Sun-bending	1.01	1.00	1.01	1.01	1.01
	St1-planet-bending	1.00	1.00	1.01	1.01	1.01
	St1-Sun-pitting	1.00	1.00	1.01	1.01	1.01
	St1-planet-pitting	1.00	1.00	1.01	1.01	1.01
Compact	PLC	0.93	0.85	0.78	0.73	0.70
	St1-PL-A	1.01	1.01	1.02	1.03	1.03
	St2-RS	1.01	1.04	1.08	1.12	1.17
	St1-Sun-bending	1.01	1.01	1.02	1.02	1.02
	St1-planet-bending	1.07	1.08	1.10	1.11	1.13
	St1-Sun-pitting	1.01	1.01	1.02	1.02	1.02

Note. Comparison of relative fatigue damage (with bending moment/without bending moment). Green value (0.5–0.8 and 1.2–1.5): low relative damage (0.3–0.5 and 1.5–3); yellow value: medium relative damage; red value (>6.0): high relative damage.

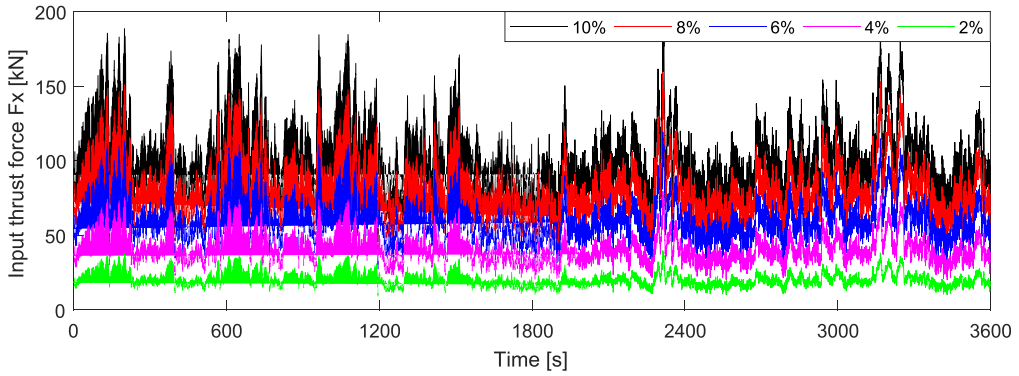

FIGURE 21 One hour time series of thrust force under five load cases [Colour figure can be viewed at wileyonlinelibrary.com]

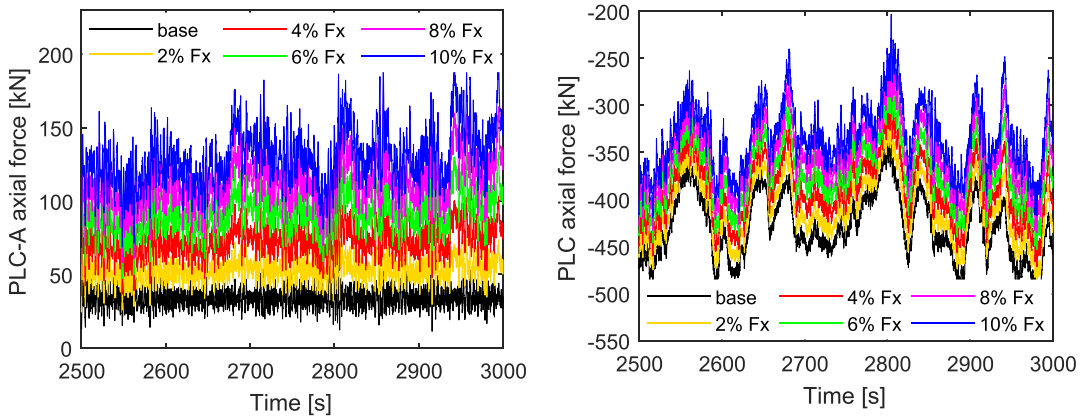

(A) PLC-A axial force (B) PLC axial force

FIGURE 22 Time series of axial force of the planet carrier bearing PLC-A in the conventional gearbox and the PLC in the compact gearbox [Colour figure can be viewed at wileyonlinelibrary.com]

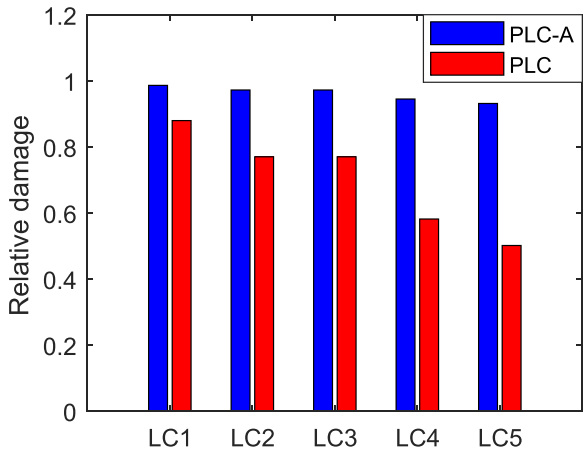

FIGURE 23 Comparison of relative damage between the PLC-A in the conventional gearbox and the PLC in the compact gearbox under all load cases [Colour figure can be viewed at wileyonlinelibrary.com]

Figure 22 presents the time series of axial force of the bearings PLC-A and PLC, respectively, under all load cases (where the base case does not consider thrust forces). It is observed that the PLC-A has a low axial force level under the base load case and it significantly increases as the applied thrust force increases, while the PLC has a large negative axial force level under the base load case and the absolute level decreases as the applied thrust force increases. The reason for this difference is related to the different gearbox layouts. In the conventional gearbox, ring gears are bolted into the gearbox housing, and the axial forces carried by the bearing PLC-A are transmitted from the planet carrier. As a contrast, in the compact gearbox, the axial forces carried by the bearing PLC are transmitted from the first stage ring gear directly because the ring gear is a rotational component. The direction of the PLC axial force is determined by the helix angle direction of the ring gear. In this model, the gear helix angle direction of the ring gear is set to produce the negative axial forces that are applied on the bearing PLC. Thus, the rotor thrust forces that are transmitted to the gearbox would be offset by the negative PLC axial forces, which is favorable for the PLC fatigue life.

Since the bearing PLC-A in the conventional gearbox and the PLC in the compact gearbox adopt a double row TRB bearing type, the applied thrust forces are mostly carried by these bearings. Figure 23 compares the relative fatigue damage of the PLC-A in the conventional gearbox and the PLC in the compact gearbox under the five thrust load cases. It is observed that the relative damage of bearing PLC is lower than the bearing PLC-A under all load cases. The relative damage of PLC decreases significantly as the thrust force increases, while a very slight decrease in the relative damage is observed in the bearing PLC-A. This can be explained by the bearing fatigue damage calculation equation, as presented in Equation 9, which shows that fatigue damage is affected by the bearing equivalent load P. In the case of the bearing PLC-A/PLC, $P = F_r$ when the ratio between the axial and radial forces is less than 0.57203, and $P = 0.5F_r + 0.57689F_a$ otherwise, based on the bearing catalogue. For the bearing PLC-A, the fatigue damage is dominated by the radial forces because its axial forces are far lower than the radial forces. In contrast, for the bearing PLC, the fatigue damage is significantly affected by the axial forces, since the ratio between the axial and radial forces is larger than 0.57203. The results in this section show that the fatigue damage of the compact gearbox is very sensitive to the thrust force, but the load effects are favorable to the gearbox fatigue life. This could also alleviate the difficulty of the main bearing design, which is one of the biggest challenges in large-scale floating wind turbines.

5 | CONCLUDING REMARKS

This study deals with a comparative analysis of the dynamic behaviour of the wind turbine gearbox between a conventional and a compact layout based on the DTU 10 MW monopile support offshore wind turbine. The two gearbox configurations are described, and their advantages and disadvantages are discussed. Load-sharing performance and fatigue damage are assessed and compared under pure torque load cases, tangential pin position error conditions and non-torque load cases. The main conclusions are summarized as follows:

- The compact gearbox has a better load-sharing performance than the conventional gearbox, especially under low torque load cases. In the first stage, the relatively poor load-sharing performance in the conventional gearbox is due to gravity effects, which do not affect the compact gearbox because its planet carrier is fixed. Additionally, the difference of the load-sharing performance in the second stage between these two gearboxes is primarily due to the differences in the floating capacity of the Sun gear in these two gearboxes.
- Because of the large floating capacity of the Sun gear in the second stage of the compact gearbox, the load-sharing performance of the compact gearbox is much less sensitive to tangential pin position error compared to the conventional gearbox.
- Compared to the gears and bearings in the compact gearbox, fatigue damage of more components is affected by the applied tangential pin position error in the conventional gearbox. Additionally, the effects of tangential pin position error on fatigue damage of components in the conventional gearbox are generally larger than those in the compact gearbox.

- Compared to the gears and bearings in the compact gearbox, fatigue damage of more components in the conventional gearbox is affected by the applied rotor pitch moments. Additionally, in general, the fatigue damage of gears and bearings in the conventional gearbox is more sensitive to the pitch moments than those in the compact gearbox, especially under severe load cases.
- Rotor thrust forces have a favorable effect on fatigue damage of the compact gearbox because they offset the axial forces of the planet carrier bearing. In contrast, the fatigue damage of the planet carrier bearing in the conventional gearbox is not sensitive to the rotor thrust force because it is more affected by radial loads.

As a whole, the present work compares a conventional and a compact gearbox model. Both are designed for the DTU 10 MW wind turbine based on an identical design methodology, in terms of weight, volume and dynamic behaviour. The study demonstrates that a lighter gearbox weight and much smaller size can be realized via the novel layout design. Additionally, in general, compared to the conventional gearbox, the compact gearbox has a better dynamic behaviour under different environmental conditions and is less vulnerable to inevitable manufacturing errors and non-torque loads. According to this study, the compact gearbox is a promising alternative for large-scale floating wind turbines. However, the assessment on gearbox performance should be conducted from a whole life cycle perspective, which includes the costs of manufacturing, installation and maintenance. Further studies on the comparison of the two gearbox performance in a whole life cycle will be conducted.

ACKNOWLEDGMENT

The first and last authors wish to acknowledge the support from the Research Council of Norway through Centre for Ships and Ocean Structures (CeSOS) and the Centre for Autonomous Marine Operations and Systems (AMOS), Norwegian University of Science and Technology. Moreover, the first author would like to thank the financial support from the China Scholarship Council (CSC) (Grant No. 201706050147).

PEER REVIEW

The peer review history for this article is available at https://publons.com/publon/10.1002/10.1002/we.2602.

ORCID

Shuaishuai Wang https://orcid.org/0000-0002-9155-9357
Amir Nejad https://orcid.org/0000-0003-0391-8696
Erin E. Bachynski https://orcid.org/0000-0002-1471-8254

REFERENCES

1. Bak C, Zahle F, Bitsche R, et al. Description of the DTU 10 MW reference wind turbine. *DTU Wind Energy Report-I-0092*; 2013.
2. Wang S, Nejad AR, Moan T. On initial design and modelling of a 10 MW medium speed drivetrain for offshore wind turbines. *J Phys Conf Ser*. 2019; 1356:12024.
3. Wang S, Nejad AR, Moan T. On design, modelling, and analysis of a 10-MW medium-speed drivetrain for offshore wind turbines. *Wind Ener*. 2020;23 (4):1099-1117.
4. Areva 5 MW wind turbine. https://en.wind-turbine-models.com/turbines/23-areva-m5000-116; 2019.
5. Vestas 9.5 MW wind turbine. https://www.modernpowersystems.com/features/featuremhi-vestas-v16-steps-up-a-gear-5886915; 2019.
6. Wang S, Nejad AR, Moan T. Design and dynamic analysis of a compact 10 MW medium speed gearbox for offshore wind turbines. *ASME J Offshore Mech Arct Eng*. 2021;143(3):32001. https://doi.org/10.1115/1.4048608
7. Guo Y, Keller J, LaCava W. Planetary gear load sharing of wind turbine drivetrains subjected to non-torque loads. *Wind Ener*. 2015;18(4):757-768.
8. Helsen J, Guo Y, Keller J. Gearbox high-speed-stage bearing slip induced by electric excitation in a test facility. *Wind Ener*. 2018;21(11):1191-1201.
9. Mo S, Zhang Y, Wu Q, Matsumura S, Houjoh H. Load sharing behavior analysis method of wind turbine gearbox in consideration of multiple-errors. *Renew Ener*. 2016;97:481-491.
10. Bhardwaj U, Teixeira AP, Soares CG. Reliability prediction of an offshore wind turbine gearbox. *Renewable Ener*. 2019;141:693-706.
11. IEC61400-4. *Wind turbines, part 4: Standard for design and specification of gearboxes*. Geneva, Switzerland: International Electrotechnical Commission; 2012.
12. ISO6336-5. *Calculation of load capacity of spur and helical gears, part 5: Strength and quality of materials*. Geneva, Switzerland: International Organization for Standardization; 2003.
13. ISO6336-2. *Calculation of load capacity of spur and helical gears, part 2: Calculation of surface durability (pitting)*. Geneva, Switzerland: International Organization for Standardization; 2006.
14. ISO6336-3. *Calculation of load capacity of spur and helical gears, part 3: Calculation of tooth bending strength*. Geneva, Switzerland: International Organization for Standardization; 2006.
15. ISO6336-6. *Calculation of load capacity of spur and helical gears, part 6: Calculation of service life under variable load*. Geneva, Switzerland: International Organization for Standardization; 2006.
16. ISO281. *Rolling bearings-dynamic load ratings and rating life*. Geneva, Switzerland: International Organization for Standardization; 2007.
17. Li L, Gao Z, Moan T. Joint distribution of environmental condition at five european offshore sites for design of combined wind and wave energy devices. *J Offshore Mech Arct Eng*. 2015;137(3):31901.
18. IEC61400-3. *Wind turbines, part 3: Design requirements for offshore wind turbines*. Geneva, Switzerland: International Electrotechnical Commission; 2009.

19. Jonkman BJ. Turbsim user's guide: Version 1.50. *tech. rep*, Golden, CO (United States), National Renewable Energy Lab.(NREL); 2009.
20. IEC61400-1. *Wind turbines, part 1: Design requirements*. Geneva, Switzerland: International Electrotechnical Commission; 2005.
21. SIMPACK. Multi-body system software. http://www.simpack.com; 2019.
22. Nejad AR, Xing Y, Guo Y, Keller J, Gao Z, Moan T. Effects of floating Sun gear in a wind turbine's planetary gearbox with geometrical imperfections. *Wind Ener*. 2015;18(12):2105-2120.
23. Wang S, Zhu C, Song C, Han H. Effects of elastic support on the dynamic behaviors of the wind turbine drive train. *Front Mech Eng-Prc*. 2017;12(3):348-356.
24. Guo Y, Keller J. Investigation of high-speed shaft bearing loads in wind turbine gearboxes through dynamometer testing. *Wind Ener*. 2018;21(2):139-150.
25. Guo Y, Keller J, La Cava W, et al. Recommendations on model fidelity for wind turbine gearbox simulations. *Tech. Rep*, Golden, CO (United States), National Renewable Energy Lab. (NREL); 2015.
26. Craig R, Bampton M. Coupling of substructures for dynamic analyses. *AIAA J*. 1968;6(7):1313-1319.
27. ISO6336-1. *Calculation of load capacity of spur and helical gears. Basic principles, introduction and general influence factors*. Geneva, Switzerland: International Organization for Standardization; 2007.
28. Dong W, Xing Y, Moan T, Gao Z. Time domain-based gear contact fatigue analysis of a wind turbine drivetrain under dynamic conditions. *Int J Fatigue*. 2013;48:133-146.
29. Jiang Z, Xing Y, Guo Y, Moan T, Gao Z. Long-term contact fatigue analysis of a planetary bearing in a land-based wind turbine drivetrain. *Wind Ener*. 2015;18(4):591-611.
30. Nejad AR, Bachynski EE, Kvittem MI, Luan C, Gao Z, Moan T. Stochastic dynamic load effect and fatigue damage analysis of drivetrains in land-based and TLP, spar and semi-submersible floating wind turbines. *Marine Struct*. 2015;42:137-153.
31. SIMA. Marine operations and mooring analysis software. https://www.dnvgl.com/services/marine-operations-and-mooring-analysis-software/-sima-2324; 2019.
32. Xing Y, Karimirad M, Moan T. Effect of spar-type floating wind turbine nacelle motion on drivetrain dynamics. In: Proceedings of European Wind Energy Association annual event (EWEA), Copenhagen, Denmark; 2012:266-275.
33. Xing Y, Karimirad M, Moan T. Modelling and analysis of floating spar-type wind turbine drivetrain. *Wind Energy*. 2014;17(4):565-587.
34. AGMA. *Design manual for enclosed epicyclic gear drives*. Alexandria, Virginia: American Gear Manufacturers Association; 2006;1-104.
35. Wilkins EWC. Cumulative damage in fatigue. In: Colloquium on Fatigue/Colloque de Fatigue/Kolloquium über Ermüdungsfestigkeit Springer, Berlin, Heidelberg; 1956:321-332.
36. Wang S, Nejad AR, Bachynski EE, Moan T. Effects of bedplate flexibility on drivetrain dynamics: Case study of a 10 MW spar type floating wind turbine. *Renew Energy*. 2020;161:808-824.
37. Nejad AR, Gao Z, Moan T. On long-term fatigue damage and reliability analysis of gears under wind loads in offshore wind turbine drivetrains. *Int J Fatigue*. 2014;61:116-128.
38. Cooley CG, Parker RG. A review of planetary and epicyclic gear dynamics and vibrations research. *Applied Mechanics Reviews*. 2014;66(4):40804.
39. Keller J, Guo Y, Zhang Z, Lucas D. Comparison of planetary bearing load-sharing characteristics in wind turbine gearboxes. *Wind Energy Sci*. 2018;3(2):947-960.
40. Austin JL. A multi-component analysis of a wind turbine gearbox using a high fidelity finite element model. *Ph.D. Thesis*; 2013.
41. Park Y-J, Lee G-H, Oh J-S, Shin C-S, Nam J-S. Effects of non-torque loads and carrier pinhole position errors on planet load sharing of wind turbine gearbox. *Int J Precision Eng Manuf-Green Technol*. 2019;6(2):281-292.
42. Guo Y, Parsons T, Dykes K, King RN. A systems engineering analysis of three-point and four-point wind turbine drivetrain configurations. *Wind Energy*. 2017;20(3):537-550.

How to cite this article: Wang S, Nejad A, Bachynski EE, Moan T. A comparative study on the dynamic behaviour of 10 MW conventional and compact gearboxes for offshore wind turbines. *Wind Energy*. 2020;1–20. https://doi.org/10.1002/we.2602